Wtip and Vangl2 are required for mitotic spindle orientation and cloaca morphogenesis

Ekaterina Bubenshchikova[1,2], Koichiro Ichimura[1,3], Yayoi Fukuyo[1], Rebecca Powell[1], Chaonan Hsu[1], Stephen O. Morrical[2], John R. Sedor[2], Tatsuo Sakai[3] and Tomoko Obara[1,2,*]

[1]Department of Cell Biology, University of Oklahoma Health Science Center, Oklahoma City, OK 73104, USA
[2]Department of Medicine and Rammelkamp Center for Education and Research, MetroHealth Medical Center, Case Western Reserve University School of Medicine, Cleveland, OH 44109, USA
[3]Department of Anatomy and Life Structure, Juntendo University School of Medicine, Tokyo 113-8421, Japan
*Author for correspondence (tomoko-obara@ouhsc.edu)

Biology Open 1, 588–596
doi: 10.1242/bio.20121016

Summary

Defects in cilia and basal bodies function are linked to ciliopathies, which result in kidney cyst formation. Recently, cell division defects have been observed in cystic kidneys, but the underlying mechanisms of such defects remain unclear. Wtip is an LIM domain protein of the Ajuba/Zyxin family, but its role in ciliogenesis during embryonic development has not been previously described. We report Wtip is enriched in the basal body and knockdown of *wtip* leads to pronephric cyst formation, cloaca malformation, hydrocephalus, body curvature, and pericardial edema. We additionally show that *wtip* knockdown embryos display segment-specific defects in the pronephros: mitotic spindle orientation defects are observed only in the anterior and middle pronephros; cloaca malformation is accompanied by a reduced number of ciliated cells; and ciliated cells lack the striated rootlet that originates from basal bodies, which results in a lack of cilia motility. Our data suggest that loss of Wtip function phenocopies Vangl2 loss of function, a core planar cell polarity (PCP) protein located in the basal body protein. Furthermore, we demonstrate that *wtip* and *vangl2* interact genetically. Taken together, our results indicate that in zebrafish, Wtip is required for mitotic spindle orientation in the anterior and middle of the pronephros, cloaca morphogenesis, and PCP, which may underlie the molecular etiology of ciliopathies.

Key words: Ciliopathies, Mitotic spindle, Basal body, Zebrafish

Introduction

Cilia are microtubule-based "hair-like" organelles that are present on the apical surface of most eukaryotic cells. Motile cilia contain a central pair of microtubules, and the basal body anchors the cilium in the cell body. The rootlet is a prominent structure that originates from the proximal end of the basal body (Yang et al., 2002). In recent years, defects in cilia and basal bodies have been linked to a number of important developmental pathways (Veland et al., 2009; Goetz and Anderson, 2010). Defects in cilia assembly and function have been causative with human ciliopathies (Harris, 2007; Hildebrandt et al., 2011). Also, it has been suggested that the basal body is involved in regulating the Wnt pathway, leading ultimately to the generation of kidney cysts (Saburi et al., 2008; Wallingford, 2010; Cao et al., 2010; Skouloudaki et al., 2009; Burcklé et al., 2011; Simons et al., 2005). However, the pathological mechanisms leading to ciliopathies remain incompletely defined.

To understand the function of the genes associated with the human ciliopathies, animal model systems have been instrumental. Many mouse and rat models of ciliopathies have been described (Harris, 2007; Hildebrandt et al., 2011; Menezes and Germino, 2009). These models share features in common with human diseases. In addition to the mammalian model systems, simple vertebrates such as zebrafish, medaka and *Xenopus* have provided an alternative, more experimentally tractable model systems to study mechanisms responsible for ciliopathies (Wessely and Obara, 2008; Swanhart et al., 2011).

Recently, evidence for the involvement of intraflagellar transport proteins (IFTs), Ofd1, and Nphp4 in Wnt-planar cell polarity (PCP) has been reported in zebrafish (Cao et al., 2010; Burcklé et al., 2011; Ferrante et al., 2009). These findings are also supported by the evidence that zebrafish maternal zygotic mutants for the core PCP gene *vangl2* lead to pronephric tubule distension and misorientation of the basal body in the neural tube and other tissues (Borovina et al., 2010). PCP signaling processes are involved in a variety of phenotypes (Goetz and Anderson, 2010; Fischer and Pontoglio, 2009; Menezes and Germino, 2009).

The WT-1-interacting protein (WTIP) was originally identified as an interacting partner of the Wilm's tumor protein 1 (WT-1) in a yeast two-hybrid screen (Srichai et al., 2004). The nuclear export signal domain (NES), the SH3 binding domain (SH3), three LIM binding domains (LIM) and the PDZ binding domain (PDZ) are encoded by *wtip*. Recent studies suggest the following: (1) Wtip interacts with the C-terminus of the receptor tyrosine kinase Ror2 in yeast and mammalian cells (Verhey van Wijk et al., 2009), and (2) Ajuba LIM proteins (Ajuba, LIMD1 and WTIP) interact with Snail to remodel epithelia dynamics (Langer

et al., 2008; Das Thakur et al., 2010). However, the subcellular localization of Wtip or its *in vivo* role during embryonic development is still unknown.

In this paper, we have used zebrafish as a model to study Wtip function during embryonic development. We show that the Wtip protein localizes in the basal body. Knockdown of *wtip* leads to pronephric cysts accompanied by cloaca malformation, hydrocephalus, body curvature and pericardial edema, all phenotypes seen in other zebrafish models of human ciliopathies. Interestingly, *wtip* knockdown embryos display segment-specific defects in the pronephros: mitotic spindle orientation defects are observed only in the anterior and middle pronephros; cloaca malformation is accompanied by fewer ciliated cells; and ciliated cells lack the striated rootlet that originates from basal bodies, resulting in a lack of cilia motility. Our data suggest that phenotypes caused by loss of Wtip are similar to defects seen in zebrafish with knockdown of the basal body protein Vangl2. We discovered that loss of *wtip* and *vangl2* act synergistically, suggesting that the phenotypes caused by loss of Wtip are due to defects in PCP signaling. We have identified new roles for Wtip in ciliopathy, namely that Wtip contributes to the connection between cystogenesis and cell division in the anterior and middle pronephros, cloaca malformation and PCP in ciliopathy.

Materials and Methods

Fish husbandry

Standard protocols were used to maintain and raise wild-type zebrafish AB strains and embryos at 28.5℃ as described by Westerfield (Westerfield, 2000). Embryos were cultured in 0.0045% phenylthiourea in a Danieau buffer to inhibit pigmentation and embryos were staged according to Kimmel et al. (Kimmel et al., 1995).

Cloning full-length of zebrafish *wtip* and *wtip* gene expression by RT-PCR

To obtain the zebrafish *wtip* gene, BLAST searches were performed using the human WTIP amino-acid sequence as the query (Srichai et al., 2004). A zebrafish full-length *wtip* cDNA clone was obtained by RT-PCR from total RNA prepared from 48 hours post fertilization (hpf) embryos using the RNAqueous®-4PCR Kit (Ambion/Life Technologies, Grand Island, New York, USA). RT-PCR was performed using the SuperScript™ III One-Step RT-PCR System with Platinum® Taq High Fidelity (Invitrogen™/Life Technologies, Grand Island, New York, USA) followed by a second PCR using Phusion® High-Fidelity DNA Polymerase (New England BioLabs, Inc., Ipswich, Massachusetts, USA). Primers used were: AAACTTTGTCACGACGGCTGTAT; ACGAGACATGATGAGGAATGACA; TCATGAATCGTGACGAAATGACT; and ACTAATTCCCGGTTTGTGGTTTT (Eurofins mwg/operon, Huntsville, Alabama, USA). The PCR product was subcloned in pCR®-BluntII-TOPO vector (Invitrogen) according to the manufacturer's instructions. RT-PCR of the *wtip* transcript was performed with total RNA isolated from 1–4 cell stages through 48 hpf embryos using the RNAqueous®-4PCR Kit (Ambion). The primers used to amplify *wtip* were: GGGATCCATGAGCGCGTATC; GAAAGGAACTCCGTCCAGACC; GTCAGGCCATCTCTGTGTTCC; and CCGGCATCAAAGATTGAAGAG (Eurofins mwg/operon). Variations in total RNA from each stage were controlled by using *gapdh.*

In situ hybridization

Whole-mount *in situ* hybridization was performed as described by Hauptmann and Gerster, (Hauptmann and Gerster, 2000), using the following probes: *wtip,* and *evx1* (Pyati et al., 2006). For the *wtip* anti-sense RNA probe, pCR®-BluntII-TOPO-*wtip* plasmid was linearized by *NotI* and SP6 RNA polymerase (Roche, Indianapolis, USA) was used to generate the DIG RNA probe. All probes were synthesized using DIG-RNA (Roche) labeling mix according to the manufacturer's instructions. Alkaline phosphatase-conjugated anti-digoxigenin (Roche) was used to localize the probes. NBT/BCIP (Roche) was used as the chromogenic substrate to produce blue.

Antibodies and whole-mount immunochemistry

A zebrafish Wtip antiserum was raised in rabbits using amino-terminal peptide CGASDRLRRYTHAEVQGHRYS coupled to KLH and the antiserum was affinity-purified against the immunizing peptide and used at 1:100 dilution (Covance, Denver, Philadelphia, USA). Other primary antibodies used included: anti-γ-tubulin (GTU-88, 1:800 dilution, Sigma, St. Louis, Missouri, USA Cat# T6557); anti-acetylated α-tubulin (6-11B-1, 1:800 dilution, Sigma Cat# T7451); anti-α-tubulin (DM1a, 1:500 dilution, Sigma Cat# T6199); anti-centrin (20H5, 1:1000 dilution, Millipore, Billerica, Massachusetts, USA Cat# 04-1624); and anti-p-Histone H3 (Ser 10) (1:750 dilution, Santa Cruz Biotechnology®, Inc., Santa Cruz, California, USA Cat# sc-8656-R). Secondary antibodies were from Molecular Probes/Invitrogen™/Life Technologies, Grand Island, New York, USA and included goat-anti-rabbit-Alexa-Fluor®546 (IgG (H+L), Cat# A11035), goat-anti-mouse-Alexa-Fluor®488 (IgG2b, Cat# A21141), goat-anti-mouse-Alexa Fluor®488 (IgG1(γ1), Cat# A21121), goat-anti-mouse-Alexa Fluor®488 (IgG2a(γ2a), Cat# A21131), and goat-anti-mouse-Alexa Fluor®546 (IgG1(γ1), Cat# A21123). Whole-mount immunochemistry was performed on embryos that were fixed in Dent's fixative (methanol: DMSO=4:1) for anti-Wtip + anti-acetylated α-tubulin, anti-Wtip + anti-γ-tubulin, anti-Wtip + anti-Centrin, anti-pH3 + anti-acetylated α-tubulin + anti-α-tubulin at 4℃ overnight. Embryos fixed by Dent's fixative or PFA/PBS fixed samples were further processed as described by Kim et al. (Kim et al., 2011). Embryos were flat-mounted and visualized using an Olympus IX81-FV500 confocal laser scanning microscope (Olympus, Center Valley, Philadelphia, USA) and analyzed with Fluo View imaging software (Olympus). An Olympus Provis AX-70 photomicroscope equipped with epifluorescence, Normaski, phase contrast optics and a Q-imaging digital camera was connected to a workstation with Q-capture software.

Morpholino and mRNA injections

The followings morpholinos were obtained from Gene Tools, LLC, Philomath, Oregon, USA: Translational blocking morpholino oligonucleotide (MO) that targeted against the 5′UTR of *wtip* (*wtipMO*: GATCCTCGTCGTATTCATCCATGTC), or the 5′UTR of *vangl2* (*vangl2MO*: GTACTGCGACTCGTTATCCATGTCG) (Cui et al., 2011): a MO that blocked splicing of *wtip* exon2 by targeting the exon 2/intron 2-3 boundary (*wtipMOex2*: TGTATTTGTAGAAACTCACCGCATG) and a randomized control MO (*conMO:* CCTCTTACCTCAGTTACAATTTATA). A volume of 4.6 nl in a concentration of 0.3 mM *wtipMO*, 2 ng/nl *vangl2MO* morpholino and 20 pg *wtip* mRNA was injected at one cell stage using a nanoliter 2000 microinjector (World Precision Instruments, Sarasota, Florida, USA). Zebrafish *wtip* mRNA were synthesized with T7 RNA polymerase (mMessage mMachine system) (Ambion), respectively after linearization of the pCR®-BluntII-TOPO®-*wtip* construct with *HindIII* (Invitrogen). All mRNA were purified using the RNeasy Mini Kit (Qiagen, Valencia, California, USA). Microinjections into 1-cell embryos were performed as described by Feng et al. (Feng et al., 2008).

Histological analysis

48 hpf embryos were fixed using histology fixative (1% paraformaldehyde, 1.5% glutaraldehyde, 3% sucrose in 70 mM phosphate buffer, (pH 7.2)) overnight at 4℃, and dehydrated by a graded series of methanol before embedding in JB4 resin according to the manufacturer's instructions (Polysciences, Inc., Warrington, Philadelphia, USA). Four micron sections were cut by a Leica RN2255 microtome (Leica, Buffalo Grove, Illinois, USA) and stained with hematoxylin and eosin (BBC Biochemical, Dallas, Texas, USA).

Electron microscopy

For transmission electron microscopy analysis, embryos were prepared by previously published protocols (Ichimura et al., 2007). Ultrathin (80–90 nm) sections were then cut and counterstained with uranyl acetate and lead citrate, and observed using a JEM-1230 transmission electron microscope (JEOL, Tokyo, Japan).

High-speed video microscopy

Minor modifications were made to a previously published protocol for high-speed video microscopy (Kramer-Zucker et al., 2005). Embryos were incubated in 75 μM phenylthiourea in Danieau buffer. 48 hpf embryos were mounted in 6% methylcellulose containing 50 mM 2,3-butanedione monoxime and 0.02% Tricane (Sigma). Images of cilia motility were taken by using a 60×/1.20 water immersion UPlanSApo DICT lens on an Olympus AX-70TRF-A microscope (Olympus) equipped with an AOS S-PRI video camera (AOS Technologies AG, El Cajon, California, USA) under a stream acquisition rate of 200 frames per second in Imaging Studio v 3.3.3 (AOS Technologies) was used. Movies were played at 7 frames per second and analyzed with VirtualDub software.

Statistical analysis

Results were analyzed by the paired Student's *t*-test. Variance is displayed as either average absolute deviation (AAD) or as SEM as noted in the figure legend. Differences were considered to be statistically significant at values of $p<0.05$; p values are as indicated by $p<0.001$.

Results

Identification and cloning of zebrafish *wtip*

Full-length zebrafish *wtip* was identified and assembled using TBLAST searches with human and mouse WTIP C-terminus sequence (including the three LIM domains) and the PDZ binding domain to identify comparable protein sequences in the zebrafish ENSEMBL database (Sanger Center). The zebrafish *wtip* gene (Ensembl gene ENSDARG00000063666) is located on chromosome 13; it contains 8 exons and encodes 648 amino acids. Zebrafish Wtip protein amino acid identity with other species ranged from 51.7 to 84.4% (human, mouse, frog, and chicken) (Fig. 1B). Notably, the coding region spanning exons 2–8 (which contains three LIM binding domains and the PDZ domain) was highly conserved. Interestingly, the N-terminal region of Wtip, which is encoded in exon1 and contains a nuclear export signal and a SH3 domain, was longer in zebrafish, frog and chicken than in human and mouse (supplementary material Fig. S1).

Expression analysis of zebrafish *wtip*

Next, we analyzed *wtip* gene expression by RT-PCR and whole-mount *in situ* hybridization at different stages of embryonic development. RT-PCR was used to detect *wtip* transcripts from 1-cell stage until 48 hpf at comparable levels (Fig. 1C). A low level of expression was detected by whole-mount *in situ* hybridization at 256-cell, 30–50% epiboly stages (data not shown). In zebrafish, the onset of zygotic transcription occurs at 512-cell stage (Westerfield, 2000), therefore we demonstrated that *wtip* mRNA is maternally deposited. From the zygote through the segmentation period, *wtip* mRNA showed weak ubiquitous expression by whole-mount *in situ* hybridization (data not shown). After 24 hpf, *wtip* expression was abundantly detected in the anterior brain, hindbrain, eye, and inner ear but low levels of expression were found in the heart and pronephros (Fig. 1F). In 48 hpf cross-sections, we confirmed punctuated *wtip* expression in the pronephric glomerulus and tubules (Fig. 1E). Zebrafish *wtip* expression in the pronephros was also confirmed by RT-PCR using total RNA prepared from isolated pronephros of 48 hpf embryos (Fig. 1D).

Zebrafish Wtip protein is localized to basal body of ciliated tissues

To further investigate how Wtip might function, we examined the subcellular localization of this protein in zebrafish using a zebrafish specific anti-Wtip antibody. Immunostaining using this Wtip antibody together with an antibody recognizing acetylated

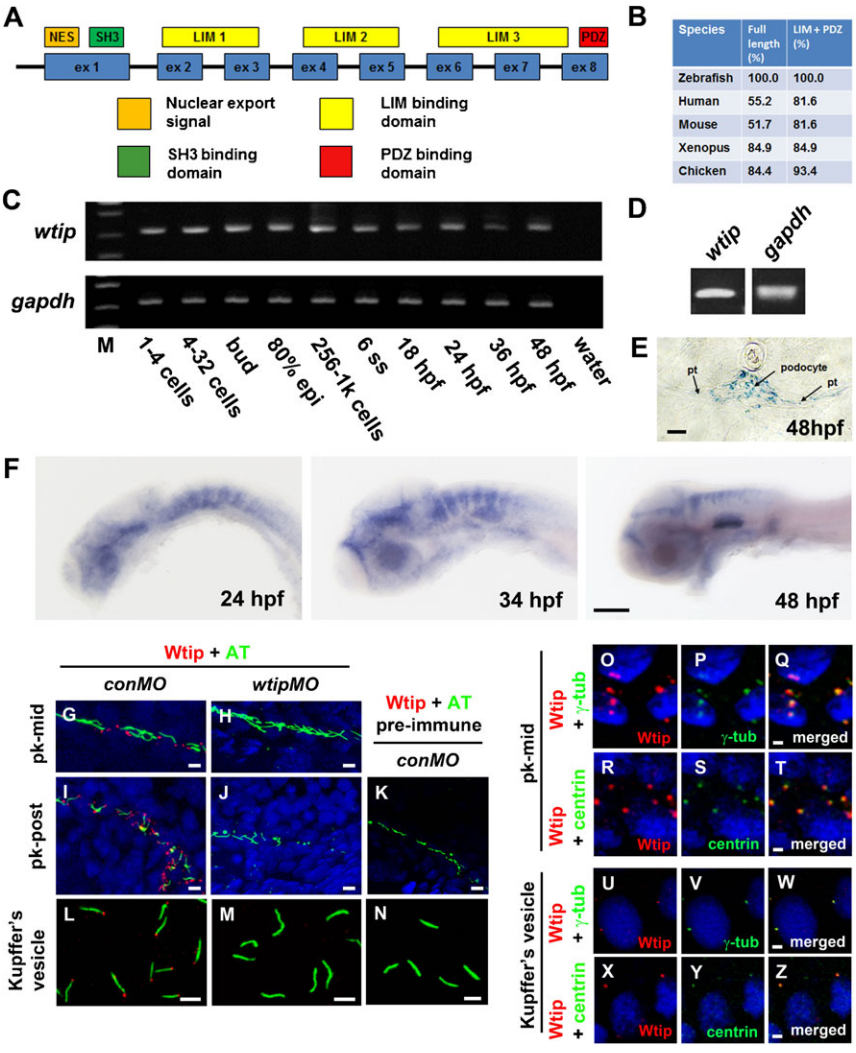

Fig. 1. Zebrafish *wtip* gene and protein during development. (**A**) Zebrafish Wtip domain structure contains one nuclear export signal (NES, orange), one SH3 binding domain (SH3, green), three LIM domains (LIM1-3, yellow) and one PDZ binding domain (PDZ, red). (**B**) Percentage of amino acid identity between zebrafish Wtip and homologs of WTIP from other species. (**C**) RT-PCR time course of *wtip* expression during embryonic development. *gapdh* was used to control variations in total RNA (**C**,**D**). *wtip* expression was maternally deposited (C) and confirmed in the pronephros by RT-PCR using total RNA from isolated pronephros from 48 hpf embryos (D). (**E**) Cross-sections of the pronephric glomerulus and tubules. (**F**) Whole-mount *in situ* hybridization for *wtip* on embryos at 24 hpf, 34 hpf, and 48 hpf are side views anterior to the left and dorsal to the top. Zebrafish *wtip* expression is restricted to the eye, anterior brain, hindbrain, inner ear, and pronephros (E,F). Double immunofluorescence for the cilia marker acetylated α-tubulin (green) and Wtip (red) in confocal projections taken from whole-mount embryos for the middle segment of the pronephros at 24 hpf (**G**,**H**), the posterior pronephros at 24 hpf (**I**,**J**,**K**) and KV at the 10-somite stage (**L**,**M**,**N**). DAPI was used to counterstain nuclei (blue). Control embryos for antibody specificity using knockdown mediated by *wtipMO* of endogeneous Wtip protein translation (H,J,M) and with pre-immune serum (K,N) showed no expression. Localization of Wtip in the basal bodies of cilia was confirmed by double immunostaining with Wtip antibody (red) and either anti-γ-tubulin (**P**,**V**, green) or anti-centrin (**S**,**Y**, green), which are basal body markers in KV (V,Y, 10-somite stage) and the middle segment of the pronephros (P,S, 24 hpf). Pronephric tubules (pt), acetylated α-tubulin antibody (AT), γ-tubulin antibody (γ-tub), mid-pronephros (pk-mid), and posterior-pronephros (pk-post). Scale bars are 10 μm in E,G–N, 100 μm in F, and 2 μm in **O**–**Z**.

α-tubulin demonstrated that the Wtip protein was localized at the base of cilia in the 24 hpf pronephros, and in Kupffer's vesicle (KV) in 10-somite stage embryos (Fig. 1G,I,L). The specificity of the staining pattern was verified by pre-incubating with immunized peptide (data not shown) or knockdown of endogeneous *wtip* expression with antisense morpholino oligonucleotide (*wtipMO*); both completely abolished the Wtip immunostaining (Fig. 1H,J,M). No staining was observed with the pre-immune serum (Fig. 1K,N). The staining pattern suggested that Wtip was localized to the basal body. To confirm this, we performed double immunostaining with two independent antibodies anti-γ-tubulin and anti-centrin. Indeed, Wtip antibody co-localized with the basal body labeled with either anti-γ-tubulin (Fig. 1O–Q,U–W) or anti-centrin (Fig. 1R–T,X–Z). Wtip was localized to the basal body of all ciliated tissues analyzed (data not shown). Together these data demonstrate that Wtip is expressed in the basal body of cilia in the ciliated tissues.

Knockdown of zebrafish *wtip* results in pronephric cysts accompanied by cloaca malformation, hydrocephalus, body curvature and pericardial edema

To address the *in vivo* function of Wtip during embryonic development, we used anti-sense morpholino (MO) mediated knockdown of *wtip (wtipMO)* to target the translational initiation site of *wtip* mRNA (Fig. 2B,E). *wtip* morphants developed pronephric cysts accompanied by cloaca malformation, hydrocephalus, body curvature, and pericardial edema (Fig. 2B,E,G,I,K). These phenotypes are highly similar to those observed for zebrafish lacking the ADPKD gene *pkd2* (Obara et al., 2006), *nphp6* (Sayer et al., 2006) and *nphp4* (Slanchev et al., 2011; Burcklé et al., 2011). Cross sections demonstrated the presence of glomerular-pronephric tubule cysts (Fig. 2G) accompanied by cloaca malformation (Fig. 2E,K) as well as dilated anterior pronephros (Fig. 2I). To assess if deletion of specific Wtip domains affects the *in vivo* functions of Wtip, we generated internal deletion allele of Wtip by disrupting mRNA splicing with a *wtip* exon2-specific donor morpholino *(wtipMOex2)* (Fig. 3A–C). Targeting the exon2 splice site donor resulted in deletion of exon2, which encodes the first Wtip LIM domain, and results in fusion of exon1 and exon3 (Fig. 3B,C). The *wtipMOex2* morphants displayed pronephric cysts accompanied by cloaca malformation, hydrocephalus, body curvature, and pericardial edema (Fig. 3D–G).

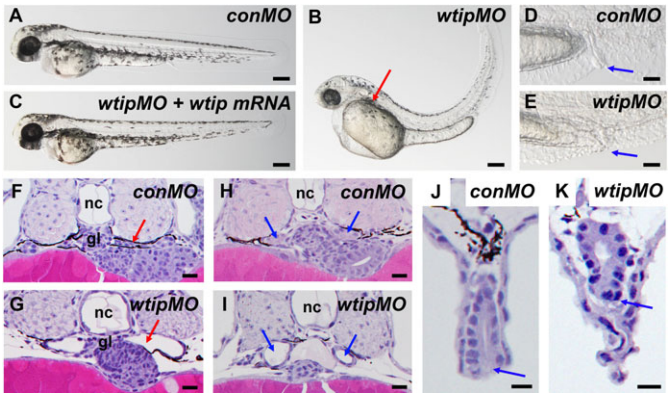

Fig. 2. *wtip* knockdown embryos show pronephric cyst formation accompanied by cloaca malformation, hydrocephalus, body axis curvature and pericardial edema. (**A,B,C**) Side view of embryos at 48 hpf under light microscopy. (B) 48 hpf *wtip* morphants form pronephric cysts, hydrocephaly, body curvature and pericardial edema. The red arrow marks the location of the cyst dilation (B). (**D,E**) Lateral view of cloaca at 48 hpf. The blue arrow marks the cloaca. (C) *wtip* mRNA can rescue pronephric cyst, body curvature, hydrocephalus, and pericardial edema caused by *wtipMO*. Histological transverse-sections of 48 hpf embryos are 4 µm JB-4 plastic sections stained with hematoxylin and eosin (**F**–**K**) at the level of the glomerulus (F,G; red arrow), anterior pronephros (H,I; blue arrow), and cloaca (J,K; blue arrow). Glomerular cysts (G), dilated anterior pronephros (I) and cloaca malformation (K) were observed in the 48 hpf *wtip* morphants. *Control* morpholino injected embryos (*conMO*), *wtip* morpholino injected embryos (*wtipMO*), glomerulus (gl), and notochord (nc). Scale bars are 200 µm in A–C, 500 µm in D,E, and 100 µm in F–K.

Importantly, the *wtipMO* or *wtipMOex2* morphants phenotype could be rescued by the co-injection of *wtip* mRNA, demonstrating that the phenotypes specifically result from *wtip* knockdown (Fig. 2C; data not shown).

It has been reported that mechanical obstruction of the cloaca generates pronephric glomerulus cysts (Kramer-Zucker et al., 2005). Recently, cloacal malformation has also been associated with pronephric cysts in other zebrafish knockdown models of ciliary gene function, including *pkd2* (Obara et al., 2006), *nphp6* (Sayer et al., 2006) and *neph4* (Burcklé et al., 2011; Slanchev et al., 2011). Indeed, we found a good correlation between the formation of pronephric glomerular cysts at 48 hpf and cloaca malformation at 24 hpf. When we observed lower concentrations of *wtip* morphants (0.5–1 ng / embryo), a normal cloaca was formed and no pronephric glomerulus cysts were developed. Conversely, higher concentrations of morpholino (4 ng / embryo) induced more severe phenotypes including the formation of pronephric glomerulus cysts accompanied by cloaca malformation. Based on these data, we decided to further analyze the specific cloacal malformation, which caused pronephric cyst formation in *wtip* knockdown zebrafish. To do so, we first determined if cloacal malformation was associated with changes in cloaca-specific gene expression. Specifically, we examined *evx1* expression by whole-mount *in situ* hybridization at 34 hpf (Fig. 4C,D), the time point when structural defects can first be seen at the gross morphological level. The *evx1* transcription factor is normally expressed in the posterior pronephros, cloaca, and ectodermal cells (Thaëron et al., 2000) (Fig. 4A,C). In the *wtip* knockdown embryos, *evx1* expression was still present in the posterior pronephros and cloaca, but the altered shape of this region was clearly marked by *evx1* expression in 34 hpf embryos (Fig. 4D). Interestingly, we found that changes in the *evx1* expression domain existed already at 24 hpf in the *wtip* morphants (Fig. 4B). At this stage *evx1* expression in *wtip* morphants has expanded towards the caudal of posterior pronephros (Fig. 4B). Together, these results suggest that Wtip is required for early caudal pronephros morphogenesis, similar to the phenotypes described in *pkd2*- (Obara et al., 2006), *nphp6*- (Sayer et al., 2006) and *nphp4*- (Slanchev et al., 2011; Burcklé et al., 2011) knockdown zebrafish. Similar to *nphp4* knockdown, we also observed in *wtip* morphants that programmed cell death of ectodermal cells that form the cloaca opening is blocked (data not shown).

Cilia formation in *wtip* morphants

Mutations in genes, which are important for cilia and basal body development, have been reported to cause pronephric cyst formation in zebrafish (Wessely and Obara, 2008; Swanhart et al., 2011). To examine the effects of *wtip* knockdown on

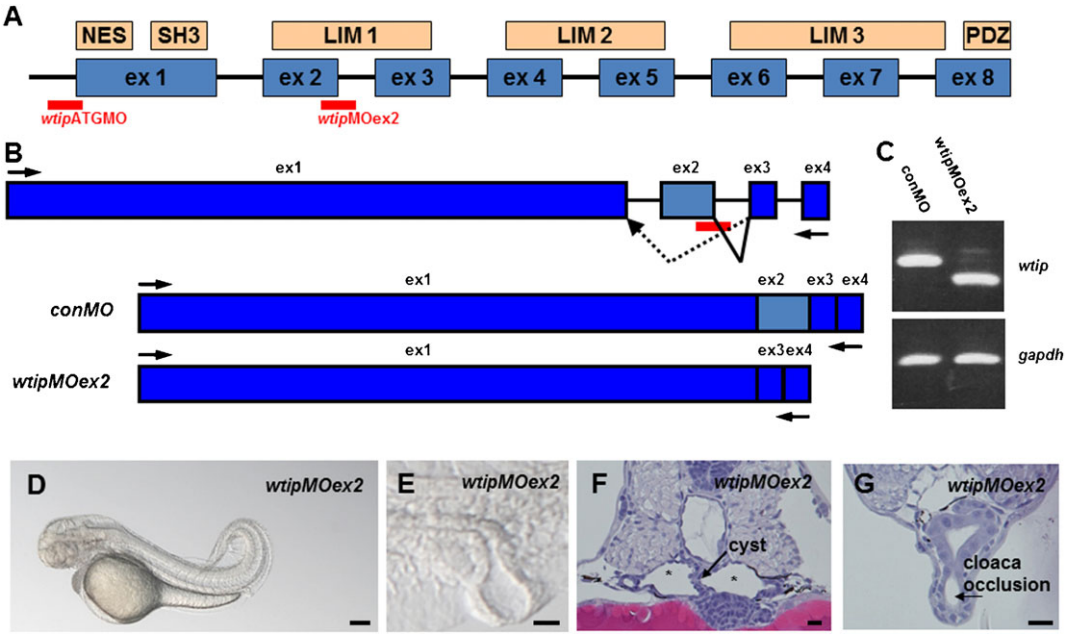

Fig. 3. Similar to *wtip* knockdown, *wtipMOex2* morphants resulted in pronephric cyst formation accompanied by cloaca malformation. (**A**) Predicted domain structure of zebrafish Wtip protein. The putative nuclear export sequence (NES), SH3 binding domains, three LIM domains and the PDZ binding domain (PDZ) are shown in boxes. Anti-sense morpholino to target the translational initiation site of *wtip* mRNA (*wtipMO*) was used for *wtip* knockdown and *wtip exon2 specific MO (wtipMOex2)* was used to target the exon2/intron2 junction. (**B**) To test the function of *wtip* in zebrafish, we targeted splice donor sites in *wtip* exon2 with MO. The extent to which steric blockade of mRNA splicing caused alterations in *wtip* mRNA processing was quantified by RT-PCR using flanking exon primers. Injection of *wtipMOex2* at the one- to two-cell stage resulted in an in-frame deletion of exon 2 and resulted in the joining of exon3 to exon1, thus deleting most of the first LIM domain. (**C**) The efficacy of the injected *wtipMOex2* was quantified at 48 hpf by RT-PCR. The upper panel shows the result of RT-PCR with primers in exons1 and 4 of *wtip*. The lower panel shows the result of RT-PCR with primers for *gapdh*, used to control RNA amounts. (**D**) Side view of 48 hpf *wtipMOex2* morphants displaying pronephric cysts, hydrocephalus, body curvature and pericardial edema. (**E**) Lateral view of cloaca at 48 hpf shows cloaca malformation. Histological transverse-sections of 48 hpf *wtipMOex2* morphant embryos are 4 μm JB-4 plastic sections stained with hematoxylin and eosin (**F**,**G**) at the level of the glomerulus cysts (F, black arrow), tubular cysts (F, asterisks) and cloaca (G, black arrow). Scale bars are 200 μm in D and 10 μm in E–G.

ciliogenesis, we examined the posterior pronephric duct by immunostaining with antibodies against the cilia marker, acetylated α-tubulin and the basal body marker γ-tubulin. As shown in Fig. 4E,F, cilia in the posterior pronephros and cloaca region of *wtip* morphants at 24 hpf were shorter than in control embryos (1.42±0.43 μm, (n=24) versus 6.31±1.23 μm, (n=32); $p<0.001$). Moreover, the number of cells forming cilia was decreased by 50% in the posterior pronephros and cloaca (Fig. 4E,F). We also examined the motility of 9+2 cilia using high-speed video microscopy analysis (supplementary material Movies 1, 2). In control 48 hpf embryos, cilia in the posterior pronephros and cloaca were motile, beating with a frequency of 63±11 Hz, n=5 (supplementary material Movie 1). By comparison, the cilia of *wtip* morphants were completely non-motile (supplementary material Movie 2).

To further understand cilia and basal body function, we examined their ultrastructure by transmission electron microscopy (Fig. 5G–I,K). In the posterior pronephros and cloaca of 34 hpf control embryos, the 9+2 axenome was associated with basal feet, transition fibers and a striated rootlet structure (Fig. 4G,I). It is noteworthy, that this unique rootlet structure (Yang et al., 2002) in the zebrafish posterior pronephros and cloaca has not been previously reported. In *wtip* morphants, the ciliated cells exhibited an intact 9+2 axenome, basal feet and transition fibers as seen in control embryos, but lacked the striated rootlet associated with the basal body (Fig. 4H,J). The remaining half of the cells in the posterior pronephros and cloaca were found to be non-ciliated cells (Fig. 4K). This is in contrast to the control embryos, where all cells were ciliated (Fig. 4I). Interestingly, in these non-ciliated cells centrosomes could still be observed, but their mother centriole/basal bodies were separated from the inner leaflet of the apical cell membrane (Fig. 4K). From these data, we conclude that Wtip is required for ciliogenesis in the posterior pronephros and cloaca. Specifically, Wtip is not required to form the 9+2 axenome, but is required for the rootlet structure, which is required for cilia motility.

Some gene products involved in human kidney diseases localized to basal bodies are known to contribute to Wnt/PCP signaling in cystic kidneys (May-Simera et al., 2010; Burcklé et al., 2011; Jonassen et al., 2008). However, phenotypic detail defects (cloaca morphogenesis, ciliogenesis) among these models are not completely identical. Therefore, we decided to examine specific defects caused by *wtip* knockdown in the posterior pronephros related to Wnt/PCP signaling. The Vangl2 protein is a core component of the PCP pathway (Ross et al., 2005). We first analyzed if *vangl2* morphants have a phenotype similar to *wtip* morphants with regard to cloaca morphogenesis, ciliogenesis and *evx1* expression pattern (Fig. 2B,E, Fig. 4B,D,F, Fig. 5A,C,E,H,K). Interestingly, *vangl2* morphants did develop cloaca malformation (Fig. 5A,C) and generated fewer cells with cilia (Fig. 5E), similar to *wtip* morphants (Fig. 2B,E,J, Fig. 4F). We next performed a combined knockdown of *wtip* and *vangl2* using sub-threshold doses of both morpholinos to assess whether a genetic interaction between these proteins would alter morphogenesis of the posterior pronephros (Fig. 5B,D). Indeed, in the *wtip* and *vangl2* double morphants, cilia were further shortened relative to controls or to *wtip*

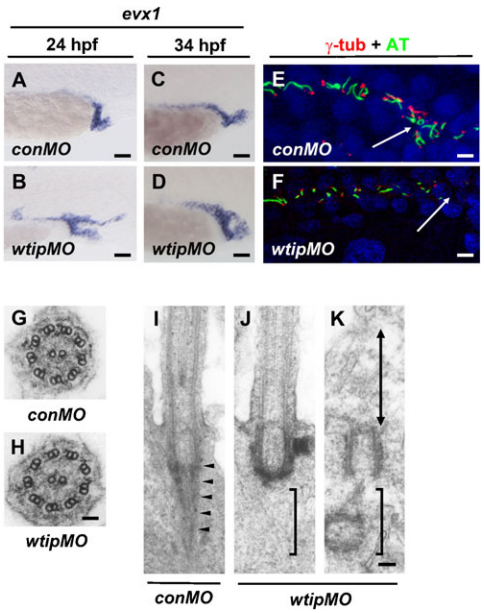

Fig. 4. In *wtip* knockdown embryos cloaca malformation is associated with fewer ciliated cells and the lack of rootlet structures, which may compromise the motility of cilia. Lateral views of *evx1* expression in control (**A**,**C**) and *wtip* morphants (**B**,**D**) in the posterior pronephros and cloaca at 24hpf (A,B) and 34 hpf (C,D). In 24 hpf (A) and 34 hpf (C) control embryos, *evx1* was expressed in the epidermis and cloaca. In *wtip* morphants, *evx1* was expressed broadly around the area of the posterior pronephros and cloaca at 24 hpf (B). *evx1* continued to be expressed at 34 hpf in the malformed cloaca (D). Confocal projections of a double immunofluorescence of the posterior pronephros and cloaca in 24 hpf control (**E**) and *wtip* morphant (**F**) embryos labeled with anti-γ-tubulin (basal body, red) and anti-acetylated α-tubulin (cilia, green) revealed fewer ciliated cell in the *wtip* morphants (F). The white arrow points to the cloaca area. Transmission electron micrographs of the transverse sections in 34 hpf control embryos (**G**) and *wtip* morphants (**H**) revealed an axoneme with 9+2 structure. Longitudinal sections in control embryos displayed a striated rootlet structure (arrowheads) located adjacent to the basal body (**I**). In *wtip* morphants, ciliated cells exhibited a basal body but lacked rootlet structure (**J**), and non-ciliated (double arrow) cells exhibited mother centrioles/basal bodies, which were separated from the inner leaflet of the apical cell membrane (**K**). Scale bars are 25 μm in A–D, 100 μm in E,F, 50 nm in G,H, and 100 nm in I–K.

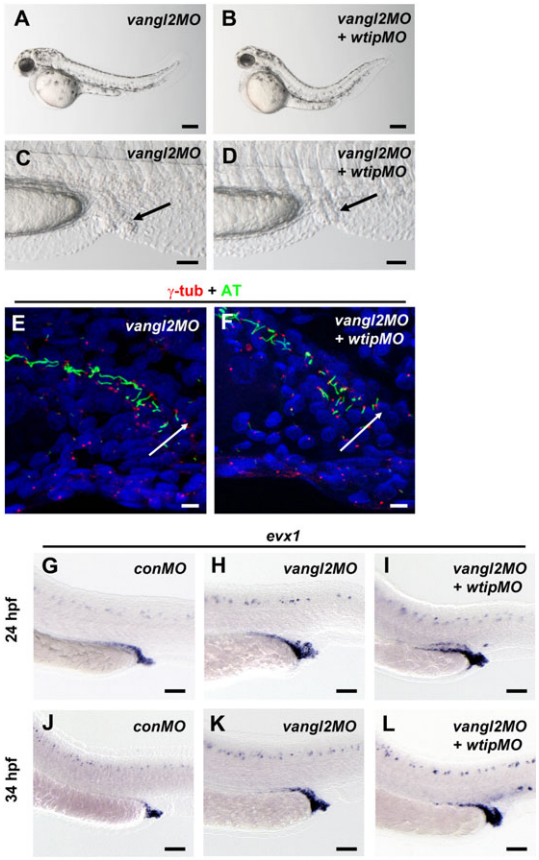

Fig. 5. In *vangl2* knockdown embryos, cloaca malformation is associated with fewer ciliated cells. (**A**,**B**) Side view of embryos at 48 hpf imaged with light microscopy. (**C**,**D**) Lateral view of cloaca at 48 hpf. The black arrow marks the cloaca. 48 hpf *vangl2* (A,C) and *vangl2* + *wtip* (B,D) morphants form pronephric cysts, cloaca malformation, hydrocephalus, body curvature and pericardial edema. Confocal projections of a double immunofluorescence of the posterior pronephros and cloaca in 24 hpf *vangl2* (**E**) and *vangl2* + *wtip* morphant (**F**) embryos labeled with anti-γ-tubulin (basal bodies, red) and anti-acetylated α-tubulin (cilia, green) revealed fewer ciliated cells in the *vangl2* (E) and *vangl2* + *wtip* morphants (F). The white arrow points to the cloaca area. Lateral views of *evx1* expression in control (**G**,**J**), *vangl2* (**H**,**K**) and *vangl2* + *wtip* morphants (**I**,**L**) in the posterior pronephros and cloaca at 24hpf (G–I) and 34 hpf (J–L). In 24 hpf (G) and 34 hpf (J) control embryos, *evx1* was expressed in the epidermis and cloaca. In *vangl2*, and *vangl2* + *wtip* morphants *evx1* was expressed broadly around the area of the posterior pronephros and cloaca at 24 hpf (H,I). *evx1* continued to be expressed at 34 hpf in the malformed cloaca (K,L). Scale bars are 200 μm in A,B, 50 μm in C,D,G–L, and 10 μm in E,F.

or *vangl2* single morphant embryos (1.05±0.43 μm, (n=18); $p<0.001$) in the posterior pronephros and cloaca at 24 hpf (Fig. 4F, Fig. 5E,F). In addition, cilia formed in 30% fewer cells in the area of the posterior pronephros and cloaca in the double *wtip* and *vangl2* knockdown embryos (Fig. 5F) as assessed by immunostaining with the cilia marker anti-acetylated α-tubulin and basal body marker anti-γ-tubulin. Finally, the expression of *evx1* in *wtip* and *vangl2* double morphants was similar to, and even more severe that in *wtip* or *vangl2* single morphant embryos at 24 and 34 hpf (Fig. 4B,D, Fig. 5H,I,K,L). The results suggest that Wtip is associated with Vangl2, and that PCP defects can influence posterior pronephros morphogenesis and ciliogenesis.

Wtip is required to maintain the correct angle of the mitotic spindle in the anterior and middle pronephros

As shown above, Wtip localizes to the basal body, and lack of Wtip results in pronephric cyst formation. One working hypothesis for the formation of PKD is that the plane of cell division is altered (Jonassen et al., 2008; Fischer and Pontoglio, 2009; Delaval et al., 2011; Jonassen et al., 2012). To test whether Wtip in zebrafish embryos affects mitotic function, *wtip* morphants were examined for spindle and cell division orientation in the 48 hpf pronephros by labeling the pronephric cilia with the anti-acetylated α-tubulin antibody and co-labeling mitotic spindle fibers with the anti-α-tubulin antibody and mitotic nuclei with the fluorescent anti-phospho Histone H3 (pH3) antibody, using an approach similar to those previously published (Toyoshima and Nishida, 2007; Delaval et al., 2011). Immunofluorescence of whole-mount zebrafish larvae at 48 hpf revealed the spindle angle relative to the cell-substrate adhesion plane. In control embryos, the spindle angle in the entire pronephros showed mitotic spindle angles of 10-20 degrees (Fig. 6A,E,I,M–O). In contrast, in *wtip* morphants, both in the anterior and the middle segments of the pronephros mitotic spindle angles ranged to up to 90 degrees (Fig. 6B,F,M,N), clearly demonstrating a critical role for Wtip in spindle orientation. Interestingly, these defects in the mitotic spindle

angles were not observed in the posterior pronephros of *wtip* morphants (Fig. 6J,O). Since the defects in the posterior pronephros of *wtip* morphants are linked to Wnt/PCP signaling, we decided to examine whether the mitotic spindle angles defects were also dependent on Wnt/PCP signaling. Like *wtip* morphants, *vangl2* morphants demonstrated mitotic spindle defects that ranged to up to 90 degrees, and again those defects were observed only in the anterior and middle but not in the posterior pronephros (Fig. 6C,G,K,M–O). This effect of the *wtip* or *vangl2* morphants was specific, since co-injection of either *wtip or vangl2* mRNA could rescue the mitotic angle defects, respectively (data not shown). We next confirmed the possible interaction of Wtip and Vangl2 through combined loss-of-function experiments using morpholinos targeting both *wtip* and *vangl2*. Embryos injected with a low dose *wtipMO* (1 ng/embryo; n=34) and *vangl2MO* (1 ng/embryo; n=28) showed no obvious defects (data not shown). However, dual knockdown of *wtip* and *vangl2* using low doses of morpholinos again perturbed the mitotic spindle angle. Indeed, the number of morphant embryos with mitotic spindle angle defects in the anterior (Fig. 6D,M) or middle pronephros (Fig. 6H,N) was increased for *wtipMO* and *vangl2MO* double morphants, but the posterior pronephros remained unaffected (Fig. 6L,O). Together, these data suggest that the two basal body proteins Wtip and Vangl2 interact and are required to establish the normal mitotic spindle angles in the anterior and middle pronephros.

Discussion

We showed in this study that, *wtip* is the first gene to be genetically linked to specific cell division phenotypes in the anterior and middle pronephros and simultaneously associated with cloaca malformation and loss of cilia motility due to their lack of rootlet structure. Moreover, we demonstrated that the non-canonical Wnt signaling pathway is required for cloacal morphogenesis, ciliogenesis and orientation of the mitotic spindles specifically in the anterior and middle pronephros. Dual knockdown of *wtip* and *vangl2* acts synergistically on kidney ciliogenesis. Importantly, the specificity of the observed phenotypes is verified by its rescue with the injection of *wtip* and *vangl2* mRNA (data not shown).

It has previously been reported that mechanical obstruction (Kramer-Zucker et al., 2005) or several zebrafish knockdown models of ciliary gene functions, including *pkd2* (Obara et al., 2006), *nphp6* (Sayer et al., 2006) and *nphp4* (Burcklé et al., 2011; Slanchev et al., 2011) of cloaca malformation resulted in pronephric cyst formation. Overall, cyst formation accompanied

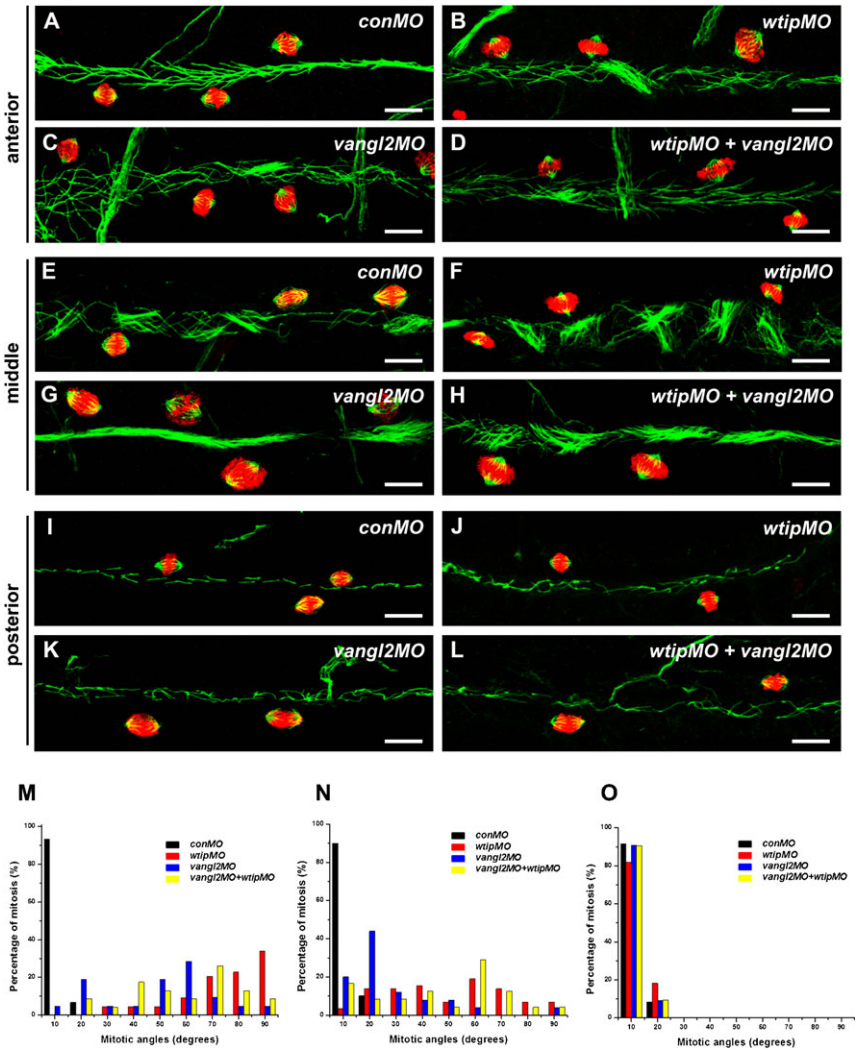

Fig. 6. *wtip* knockdown leads to mitotic cell division defects in the pronephros. Whole-mount immunofluorescence of mitotic spindles for the 48 hpf pronephros were stained with anti-acetylated α-tubulin (cilia, green), anti-α-tubulin (spindle, green) and anti-phosphorylated histone H3 (pH3, red) for the anterior (**A–D**), middle (**E–H**) and posterior (**I–L**) pronephros. In control embryos, cells with mitotic spindle fibers oriented in the longitudinal plane of the anterior (A), middle (E) and posterior (I) pronephros. In the anterior (A–D) and middle (E–H) pronephros, *wtip* morphants (B,F,J), *vangl2* morphants (C,G,K) and *wtip* + *vangl2* morphants (D,H,L) resulted in mitotic spindle orientation defects. The posterior pronephros (I–K) showed mitotic spindles oriented normally in the longitudinal plan (I–L). Mitotic spindle angles were photographed by confocal imaging in the three segments of the anterior (A–D,**M**), middle (E–H,**N**) and posterior (I–L,**O**) pronephros at 48 hpf. The angle between the long axis of the pronephros and the spindle fibers was measured; angles were grouped into 10 degree bins. Scale bars are 100 μm in A–L.

by cloaca malformation is usually explained as a result of impaired fluid excretion from the cloaca. However, the details of morphogenesis and ciliogenesis in the caudal pronephros, such as number of ciliated cells, cilia motility, and cilia structure defects leading to pronephric cysts, differ in each case. In *pkd2* (Obara et al., 2006; unpublished) and *nphp6* (Sayer et al., 2006) knockdown, no defects were observed in cilia length and cilia motility in cloaca. In *nphp4* knockdown, pronephric ducts displayed increased cell number, shorter cilia length, slower cilia motility in cloaca and programmed cell death of ectodermal cells forming the cloaca opening failed to occur (Burcklé et al., 2011; Pyati et al., 2006). In the case of Wtip, our results show that it is localized to the basal body and that its contribution to cloacal ciliogenesis is different from that reported in previous research (Obara et al., 2006; Sayer et al., 2006; Burcklé et al., 2011; Slanchev et al., 2011). We demonstrated that cloaca defects by morpholino targeting ATG site *(wtipMO)* and also *wtip* exon2 for deletion via a splice blocking morpholino *(wtipex2MO)* which lacks part of the first LIM domain, suggesting that the Wtip LIM1 domain is essential to maintain the number of ciliated cells in the posterior pronephros and cloaca. Prior to the gross cloaca morphogenesis defects demonstrated at 34 hpf, the pattern of cloaca-specific gene *(evx1)* expression was altered from 24 hpf in *wtip* knockdown zebrafish. The basal body structure was not affected in *wtip* knockdown. However, the rootlet structure normally connected to the basal body was never formed in ciliated cells of cloaca and the 9+2 cilia were non-motile. By contrast, the number of ciliated cells and cilia motility were unaffected in the anterior and middle segment of pronephros, which indicated that the role of Wtip is specific to the pronephros segments. Furthermore, other cystic genes such as *ift88* knockdown and mutants (unpublished data) display no cloaca malformation despite glomerulus cysts, body curvature, hydrocephalus and pericardial edema. This suggests that cystogenesis may proceed independently from defects in caudal pronephros (Kramer-Zucker et al., 2005; Burcklé et al., 2011; Slanchev et al., 2011).

Recent studies indicate that PCP is regulated by the non-canonical Wnt pathway and that some of the proteins involved in human kidney cystic diseases localized to the basal body are known to contribute to Wnt/PCP signaling (May-Simera et al., 2010; Burcklé et al., 2011; Jonassen et al., 2008). PCP core protein Vangl2 is known to localize to the basal body (Ross et al., 2005) and our results demonstrated that Wtip localized to the basal body is a maternal gene product. Therefore, we examined whether specific defects caused by *wtip* knockdown in the caudal pronephros are related to Wnt/PCP signaling. Interestingly, *vangl2* morphants do develop cyst formation accompanied by cloaca malformation and generate fewer ciliated cells, a phenotype strikingly similar to that of *wtip* morphants. The involvement of additional mechanisms in cyst formation in *wtip* knockdown is further supported by functional interaction experiments, in which *vangl2* knockdown dramatically enhances pronephric cyst formation accompanied by cloaca malformation.

Our results showed that the basal body protein Wtip plays segment-specific roles in the pronephros. Our working hypothesis regarding cystic kidneys is that the plane of cell division may be altered in *wtip* knockdown. Recently, it has been noted that in cystic kidneys, mitotic spindles along the tubules fail to form a proper orientation; however, the contribution of misaligned cell division to cystic kidneys remains unclear (Jonassen et al., 2008; Jonassen et al., 2012; Fischer and Pontoglio, 2009). Due to the simple structure of the zebrafish pronephros, in contrast to the mouse, we were able to analyze the mitotic spindle formation in the same nephron in a segment-specific manner, from the anterior to posterior pronephros, during the different embryonic developmental stages which had thus far remained elusive in zebrafish ciliary knockdown. In the anterior and middle pronephros, *wtip* knockdown failed to properly orient the mitotic spindles along the tubules. Interestingly, *vangl2MO* synergistically enhanced *wtipMO* mitotic spindle defects only in the anterior and middle pronephros and resulted in fewer ciliated cells in the cloaca. Therefore, we demonstrated for the first time that the signaling of the core PCP protein Vangl2 is required for proper mitotic orientation along the tubules in the anterior and middle segment of the pronephros and for the number of ciliated cells in the posterior pronephros. The exact relationship of Vangl2 and Wtip is unclear at present but they may govern apical actin assembly and migration of the centrosome during early cell polarization which is a crucial step for cilia formation. Our data suggest that it will be interesting to determine whether this phenotype may be extrapolated to other cystic genes that are studied in zebrafish, other animal models, and human ciliopathies.

Another possible model of Wtip function is that its cell-type specific actions may specifically affect fluid flow in the middle of pronephros, where we speculate that Wtip is affecting cell fate (unpublished). One main advantage of the zebrafish model is its optical translucency, which facilitates live imaging of the cellular processes underlying morphogenesis. In particular, it will be interesting to verify the Wtip protein localization in a cell type specific manner during the different developmental stages and conduct the noninvasive observation of morphogenetic processes in real time to develop early detection markers for human disease.

The present study introduces Wtip as a new player in kidney development and ciliopathy. Furthermore, this work will help to determine, whether we can utilize zebrafish as a novel target for therapeutic intervention in ciliopathy, diseases for which there are currently no approved treatments beyond supportive care.

Acknowledgements

We would like to thank Drs Deborah Garrity, Oliver Wessely, Hiroyuki Matsumoto, Brian Ceresa, and Larry Rothblum for critical reading of the manuscript. We would like to thank Drs I. A. Drummond, J. Chen, Z. Sun, N. Pathak, Y. Liu, D. Kimelman, R. D. Burdine, D. M. Garrity and A. Davidson for plasmid DNAs, zebrafish transgenic lines and mutants. We acknowledge the Zebrafish Information Resource Center (ZIRC) for providing fish. T.O. acknowledges financial support from the University of Oklahoma Health Science Center (OUHSC) and MetroHealth Medical Center. This work was supported by NIH R21-DK069604 (T.O.), NIH R01-DK078209 (T.O.), PKD foundation (69a2r) (T.O.), and R01-DK064719 (J.R.S.). This work was supported in part by funds from DMEI/NEI Image Acquisition Core Facility at the OUHSC (NIH: P30-EY12190, COBRE-P20 RR017703) and Diabetes Histology and Image Acquisition and Analysis Core Facility at OUHSC (NIH: COBRE-1P20RR024215).

Competing Interests

The authors declare that there are no competing interests.

References

Borovina, A., Superina, S., Voskas, D. and Ciruna, B. (2010). Vangl2 directs the posterior tilting and asymmetric localization of motile primary cilia. *Nat. Cell Biol.* **12**, 407-412.

Burcklé, C., Gaudé, H. M., Vesque, C., Silbermann, F., Salomon, R., Jeanpierre, C., Antignac, C., Saunier, S. and Schneider-Maunoury, S. (2011). Control of the Wnt pathways by nephrocystin-4 is required for morphogenesis of the zebrafish pronephros. *Hum. Mol. Genet.* **20**, 2611-2627.

Cao, Y., Park, A. and Sun, Z. (2010). Intraflagellar transport proteins are essential for cilia formation and for planar cell polarity. *J. Am. Soc. Nephrol.* **21**, 1326-1333.

Cui, S., Capecci, L. M. and Matthews, R. P. (2011). Disruption of planar cell polarity activity leads to developmental biliary defects. *Dev. Biol.* **351**, 229-241.

Das Thakur, M., Feng, Y., Jagannathan, R., Seppa, M. J., Skeath, J. B. and Longmore, G. D. (2010). Ajuba LIM proteins are negative regulators of the Hippo signaling pathway. *Curr. Biol.* **20**, 657-662.

Delaval, B., Bright, A., Lawson, N. D. and Doxsey, S. (2011). The cilia protein IFT88 is required for spindle orientation in mitosis. *Nat. Cell Biol.* **13**, 461-468.

Feng, S., Okenka, G. M., Bai, C. X., Streets, A. J., Newby, L. J., DeChant, B. T., Tsiokas, L., Obara, T. and Ong, A. C. (2008). Identification and functional characterization of an N-terminal oligomerization domain for polycystin-2. *J. Biol. Chem.* **283**, 28471-28479.

Ferrante, M. I., Romio, L., Castro, S., Collins, J. E., Goulding, D. A., Stemple, D. L., Woolf, A. S. and Wilson, S. W. (2009). Convergent extension movements and ciliary function are mediated by ofd1, a zebrafish orthologue of the human oral-facial-digital type 1 syndrome gene. *Hum. Mol. Genet.* **18**, 289-303.

Fischer, E. and Pontoglio, M. (2009). Planar cell polarity and cilia. *Semin. Cell Dev. Biol.* **20**, 998-1005.

Goetz, S. C. and Anderson, K. V. (2010). The primary cilium: a signalling centre during vertebrate development. *Nat. Rev. Genet.* **11**, 331-344.

Harris, P. C. (2007). Genetic complexity in Joubert syndrome and related disorders. *Kidney Int.* **72**, 1421-1423.

Hauptmann, G. and Gerster, T. (2000). Multicolor whole-mount in situ hybridization. *Methods Mol. Biol.* **137**, 139-148.

Hildebrandt, F., Benzing, T. and Katsanis, N. (2011). Ciliopathies. *N. Engl. J. Med.* **364**, 1533-1543.

Ichimura, K., Kurihara, H. and Sakai, T. (2007). Actin filament organization of foot processes in vertebrate glomerular podocytes. *Cell Tissue Res.* **329**, 541-557.

Jonassen, J. A., San Agustin, J., Follit, J. A. and Pazour, G. J. (2008). Deletion of IFT20 in the mouse kidney causes misorientation of the mitotic spindle and cystic kidney disease. *J. Cell Biol.* **183**, 377-384.

Jonassen, J. A., Sanagustin, J., Baker, S. P. and Pazour, G. J. (2012). Disruption of IFT Complex A Causes Cystic Kidneys without Mitotic Spindle Misorientation. *J. Am. Soc. Nephrol.* **23**, 641-651.

Kim, S., Zaghloul, N. A., Bubenshchikova, E., Oh, E. C., Rankin, S., Katsanis, N., Obara, T. and Tsiokas, L. (2011). Nde1-mediated inhibition of ciliogenesis affects cell cycle re-entry. *Nat. Cell Biol.* **13**, 351-360.

Kimmel, C. B., Ballard, W. W., Kimmel, S. R., Ullmann, B. and Schilling, T. F. (1995). Stages of embryonic development of the zebrafish. *Dev. Dyn.* **203**, 253-310.

Kramer-Zucker, A. G., Olale, F., Haycraft, C. J., Yoder, B. K., Schier, A. F. and Drummond, I. A. (2005). Cilia-driven fluid flow in the zebrafish pronephros, brain and Kupffer's vesicle is required for normal organogenesis. *Development* **132**, 1907-1921.

Langer, E. M., Feng, Y., Zhaoyuan, H., Rauscher, F. J., 3rd, Kroll, K. L. and Longmore, G. D. (2008). Ajuba LIM proteins are snail/slug corepressors required for neural crest development in Xenopus. *Dev. Cell* **14**, 424-436.

May-Simera, H. L., Kai, M., Hernandez, V., Osborn, D. P., Tada, M. and Beales, P. L. (2010). Bbs8, together with the planar cell polarity protein Vangl2, is required to establish left-right asymmetry in zebrafish. *Dev. Biol.* **345**, 215-225.

Menezes, L. F. and Germino, G. G. (2009). Polycystic kidney disease, cilia, and planar polarity. *Methods Cell Biol.* **94**, 273-297.

Obara, T., Mangos, S., Liu, Y., Zhao, J., Wiessner, S., Kramer-Zucker, A. G., Olale, F., Schier, A. F. and Drummond, I. A. (2006). Polycystin-2 immunolocalization and function in zebrafish. *J. Am. Soc. Nephrol.* **17**, 2706-2718.

Pyati, U. J., Cooper, M. S., Davidson, A. J., Nechiporuk, A. and Kimelman, D. (2006). Sustained Bmp signaling is essential for cloaca development in zebrafish. *Development* **133**, 2275-2284.

Ross, A. J., May-Simera, H., Eichers, E. R., Kai, M., Hill, J., Jagger, D. J., Leitch, C. C., Chapple, J. P., Munro, P. M., Fisher, S. et al. (2005). Disruption of Bardet-Biedl syndrome ciliary proteins perturbs planar cell polarity in vertebrates. *Nat. Genet.* **37**, 1135-1140.

Saburi, S., Hester, I., Fischer, E., Pontoglio, M., Eremina, V., Gessler, M., Quaggin, S. E., Harrison, R., Mount, R. and McNeill, H. (2008). Loss of Fat4 disrupts PCP signaling and oriented cell division and leads to cystic kidney disease. *Nat. Genet.* **40**, 1010-1015.

Sayer, J. A., Otto, E. A., O'Toole, J. F., Nurnberg, G., Kennedy, M. A., Becker, C., Hennies, H. C., Helou, J., Attanasio, M., Fausett, B. V. et al. (2006). The centrosomal protein nephrocystin-6 is mutated in Joubert syndrome and activates transcription factor ATF4. *Nat. Genet.* **38**, 674-681.

Simons, M., Gloy, J., Ganner, A., Bullerkotte, A., Bashkurov, M., Krönig, C., Schermer, B., Benzing, T., Cabello, O. A., Jenny, A. et al. (2005). Inversin, the gene product mutated in nephronophthisis type II, functions as a molecular switch between Wnt signaling pathways. *Nat. Genet.* **37**, 537-543.

Skouloudaki, K., Puetz, M., Simons, M., Courbard, J. R., Boehlke, C., Hartleben, B., Engel, C., Moeller, M. J., Englert, C., Bollig, F. et al. (2009). Scribble participates in Hippo signaling and is required for normal zebrafish pronephros development. *Proc. Natl. Acad. Sci. USA* **106**, 8579-8584.

Slanchev, K., Pütz, M., Schmitt, A., Kramer-Zucker, A. and Walz, G. (2011). Nephrocystin-4 is required for pronephric duct-dependent cloaca formation in zebrafish. *Hum. Mol. Genet.* **20**, 3119-3128.

Srichai, M. B., Konieczkowski, M., Padiyar, A., Konieczkowski, D. J., Mukherjee, A., Hayden, P. S., Kamat, S., El-Meanawy, M. A., Khan, S., Mundel, P. et al. (2004). A WT1 co-regulator controls podocyte phenotype by shuttling between adhesion structures and nucleus. *J. Biol. Chem.* **279**, 14398-14408.

Swanhart, L. M., Cosentino, C. C., Diep, C. Q., Davidson, A. J., de Caestecker, M. and Hukriede, N. A. (2011). Zebrafish kidney development: basic science to translational research. *Birth Defects Res. C Embryo Today* **93**, 141-156.

Thaëron, C., Avaron, F., Casane, D., Borday, V., Thisse, B., Thisse, C., Boulekbache, H. and Laurenti, P. (2000). Zebrafish *evx1* is dynamically expressed during embryogenesis in subsets of interneurones, posterior gut and urogenital system. *Mech. Dev.* **99**, 167-172.

Toyoshima, F. and Nishida, E. (2007). Integrin-mediated adhesion orients the spindle parallel to the substratum in an EB1- and myosin X-dependent manner. *EMBO J.* **26**, 1487-1498.

Veland, I. R., Awan, A., Pedersen, L. B., Yoder, B. K. and Christensen, S. T. (2009). Primary cilia and signaling pathways in mammalian development, health and disease. *Nephron Physiol.* **111**, 39-53.

Verhey van Wijk, N., Witte, F., Feike, A. C., Schambony, A., Birchmeier, W., Mundlos, S. and Stricker, S. (2009). The LIM domain protein Wtip interacts with the receptor tyrosine kinase Ror2 and inhibits canonical Wnt signalling. *Biochem. Biophys. Res. Commun.* **390**, 211-216.

Wallingford, J. B. (2010). Planar cell polarity signaling, cilia and polarized ciliary beating. *Curr. Opin. Cell Biol.* **22**, 597-604.

Wessely, O. and Obara, T. (2008). Fish and frogs: models for vertebrate cilia signaling. *Front. Biosci.* **13**, 1866-1880.

Westerfield, M. (2000). *The Zebrafish Book: A Guide For The Laboratory Use Of Zebrafish Danio (Brachydanio) Rerio*. Eugene, OR, USA: University of Oregon Press.

Yang, J., Liu, X., Yue, G., Adamian, M., Bulgakov, O. and Li, T. (2002). Rootletin, a novel coiled-coil protein, is a structural component of the ciliary rootlet. *J. Cell Biol.* **159**, 431-440.